PNAS RESEARCH ARTICLE | EARTH, ATMOSPHERIC, AND PLANETARY SCIENCES OPEN ACCESS

Cyclone Jasper's rains in the context of climate change

Kerry Emanuel[a,1]

Contributed by Kerry Emanuel; received January 6, 2024; accepted February 2, 2024; reviewed by Michael Mann and Hamish A. Ramsay

Cyclone Jasper struck northern Queensland in mid-December, 2023, causing extensive flooding stemming from torrential rain. Many stations reported rainfall totals exceeding 1 m, and a few surpassed 2 m, possibly making Jasper the wettest tropical cyclone in Australian history. To be better prepared for events like Jasper, it is useful to estimate the probability of rainfall events of Jasper's magnitude and how that probability is likely to evolve as climate warms. To make such estimates, we apply an advanced tropical cyclone downscaling technique to nine global climate models, generating a total of 27,000 synthetic tropical cyclones each for the climate of the recent past and that of the end of this century. We estimate that the annual probability of 1 m of rain from tropical cyclones at Cairns increases from about 0.8% at the end of the 20th century to about 2.3% at the end of the 21st, a factor of almost three. Interpolating frequency to the year 2023 suggests that the current annual probability of Jasper's rainfall is about 1.2%, about a 50% increase over that of the year 2000. Further analysis suggests that the primary causes of increasing rainfall are stronger cyclones and a moister atmosphere.

tropical cyclones | flooding | climate change

Significance

Flooding is a major source of mortality and damage in tropical cyclones, and over time, the bulk of these deleterious effects are contributed by extreme, low-probability events. Cyclone Jasper, which affected Queensland, Australia, in mid-December, 2023, is an example of such an event, perhaps the wettest tropical cyclone in Australian history. Here, we apply advanced physical modeling techniques to estimate the likelihood of rainfall as large as that observed in Jasper. This suggests that the probability of such intense rain near Cairns has increased by 50% since the year 2000 and is likely to double from now until the end of this century.

Cyclone Jasper developed in the Solomon Islands region in early December and, moving southwestward, intensified to a high-end Category four severe tropical cyclone by December 8th. Jasper weakened thereafter but intensified again before making landfall near the Queensland town of Wujal Wujal (~170 km north of Cairns) on 13 December, with 10-min winds estimated at 95 km/h. Cyclone Jasper stalled over the Cape York peninsula and tracking stopped after 18 December. The track of Cyclone Jasper is displayed in Fig. 1.

While the region suffered little wind damage, torrential rains persisting for as long as 5 d caused extensive flooding, with preliminary damage estimates of AU$1 billion (1). Rainfall totals over the 5 d from December 14th to 18th (Fig. 2) approached and may have exceeded 2 m in some locations; e.g., Kuranda Railway Station recorded 1.9 m while nearly 2.1 m was recorded at Whyanbeel Valley.* If these rainfall totals are verified, Jasper could well be the wettest cyclone in Australian history. The Daintree River rose more than 2 m higher than the previous 118-y-old flood level, set in 2019 (2).

It is of both scientific and practical interest to estimate the probability of tropical cyclone rainfall, and how that probability is evolving as climate changes. Here we estimate the current and future annual probability of rainfall at the city of Cairns, Australia, using an advanced tropical cyclone downscaling technique, described in the next section.

1. Data and Methods

There are too few reliable records of tropical cyclones in the Australian region to serve as a robust estimate of historical risk, and even if there were, climate has changed enough in recent decades to render historical records somewhat obsolete as a guide to current tropical cyclone risk. For this reason, we turn to models to estimate both current and future risk.

While global climate models are useful for simulating large-scale climate and climate change, they are far too coarse to simulate tropical cyclones with any fidelity. (The best resolution in current models entails grid spacings of around 50 km, capable, at best, of resolving features with scales of around 200 km. Yet, the all-important inner cores of tropical cyclones have scales of around 100 km or less.) For this reason, and to produce a far larger set of storms than can be simulated with global models, we use the downscaling method developed by the author and his colleagues (3, 4). Tropical cyclone genesis is initiated by seeding randomly, in time and space, the time-evolving large-scale environment provided by global climate models or reanalyses. The large-scale environment is represented by Fourier series in time with random phase, constrained so that the monthly means of all variables and the monthly mean variances and covariances among the wind

*As of this writing, these storm total rainfall amounts are preliminary estimates, downloaded from the Bureau of Meteorology's website, http://www.bom.gov.au/climate/data/.

Author affiliations: [a]Lorenz Center, Massachusetts Institute of Technology, Cambridge, MA 02139

Author contributions: K.E. designed research; performed research; contributed new analytic tools; analyzed data; and wrote the paper.

Reviewers: M.M., University of Pennsylvania; and H.A.R., Commonwealth Scientific and Industrial Research Organisation.

Competing interest statement: K.E. is a board member of Plymouth Rock Home Insurance and TRU insurance and is the chief scientific officer of WindRiskTech, LLC, which provides tropical cyclone risk estimates.

[1]Email: emanuel@mit.edu.

Published April 1, 2024.

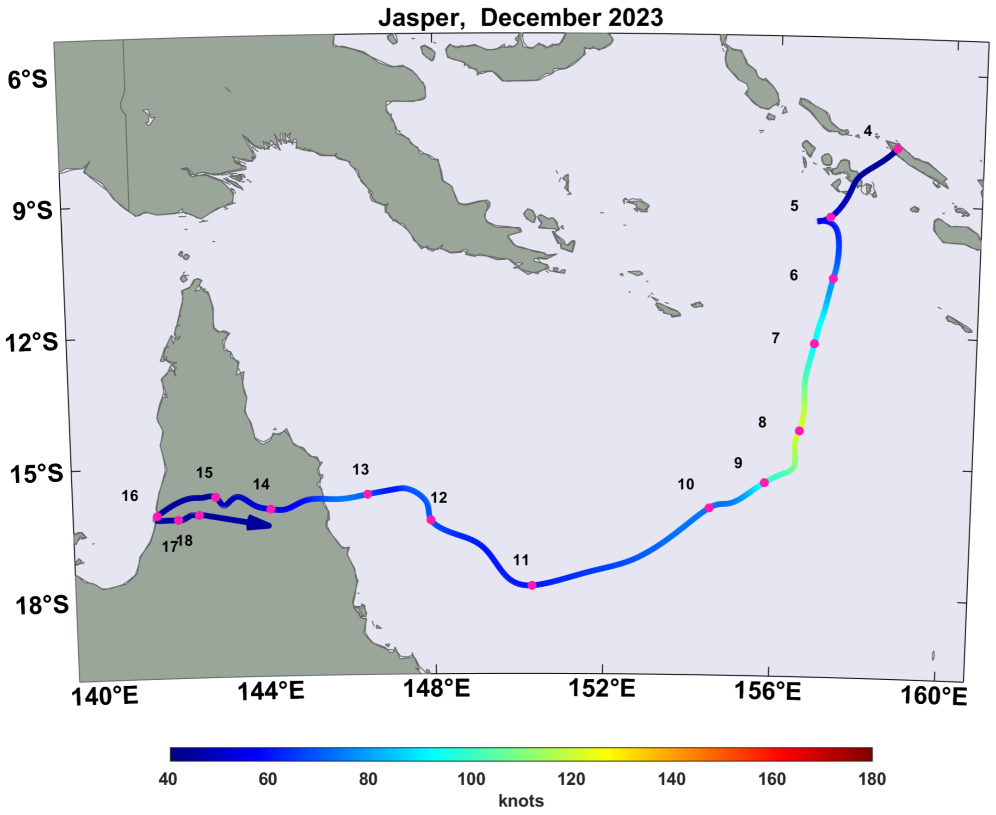

Fig. 1. Track of the center of Cyclone Jasper. Red dots show 00 GMT positions, labeled by dates in December, 2023. The color along the track show estimated peak 1-min winds according to the scale at bottom.

components are identical to those of the gridded data. The kinetic energy spectrum of the synthesized large-scale winds is also constrained to obey geostrophic turbulence scaling. The synthetic time series are then bilinearly interpolated to the storm positions and linearly interpolated to the date and time.

A tropical cyclone intensity model (CHIPS; 5) is then run along each of the randomly generated tracks. Owing to the use of an angular momentum radial coordinate, the intensity model has very high spatial resolution in the storm core. It has been shown to produce skillful real-time intensity forecasts (5). Over 99% of the seeded tracks dissipate and are discarded; the survivors are regarded as constituting the tropical cyclone climatology of the original reanalysis or climate model. When applied to global reanalysis data, this technique has been shown to accurately simulate all the salient features of the current climatology of tropical cyclones (4).

The ratio of the number of initial seeds that develop into tropical cyclones to the total number of seeds deployed is a measure of the overall frequency of the synthetic tropical cyclones. To calibrate the historical period event sets, we multiply this ratio by a single scalar so that the total rate of synthetic tropical cyclones matches that derived from historical tropical cyclone data (6). This same calibration constant is applied to future event sets.

This technique has several advantages over conventional downscaling using regional models. The use of angular momentum coordinates allows for increasing spatial resolution of the storm core as its intensity increases; consequently, each storm's intensity is limited by the physical properties of its environment rather than by numerical resolution. Because the tropical cyclone model is driven by the statistics of the global model or reanalysis, an arbitrarily large number of events can be simulated in a given climate.

Tropical cyclone rainfall is generated by a post-processing technique applied every 2 h to each track. The technique applies quasi-balanced dynamics to the interaction of the tropical cyclone with the surface and with the surrounding atmospheric environment and includes effects of surface friction, with variable surface roughness, topography, cyclone dynamics, and interaction of the cyclone with sheared atmospheric flow and humidity. The algorithm has been thoroughly tested against both radar and rain gauge data in the United States (7).

This downscaling technique has been applied in a wide variety of wind risk and storm surge studies (e.g., refs. 8 and 9–18) and studies of freshwater flood hazards (7, 13, 16, 19–22).

Here, we downscale ERA5 reanalyses (23) and 9 CMIP6-generation global climate models: The Canadian Centre for Climate Modelling and Analysis CanESM5, the EC-Earth consortium EC-Earth3, the Institut Pierre Simon Laplace IPSL-CM6A-LR, the MIROC6 model of the Center for Climate System Research, the University of Tokyo, the Japan Agency for Marine-Earth Science and Technology, and the National Institute for Environmental Studies; the Max Planck Institute MPI-ESM1-2-HR, the Japanese Meteorological Institute MRI-ESM2-0, the Norwegian Climate Center NORESM2-LM, and the United Kingdom Meteorological Office UKESM1-0-LL.

For the present purpose, we generated tracks each of which passes within 150 km of Cairns with maximum 1-min surface winds of at least 35 kts (65 km/h). From the ERA5 reanalysis, we generated 4,300 tropical cyclone events over the period 1980 to 2022, while for the climate models, we generated 3,000 tracks for each of the nine climate models for each of two periods: 1985 to 2014 from the historical simulations and 2071 to 2100 from socio-economic pathway SSP3-7.0, for a total of 54,000 tracks from the climate models.

The overall frequency of the ERA5 and global climate model historical downscalings is calibrated to the observed frequency of cyclones passing within 150 km of Cairns with maximum 1-min surface winds of at least 35 kts (65 km/h) over the period 1950 to 2022. (We use a longer period here than we use in the downscaling to obtain a more robust frequency estimate.) The annual frequency of observed events is about 0.2. The same multiplicative factor derived for each of the

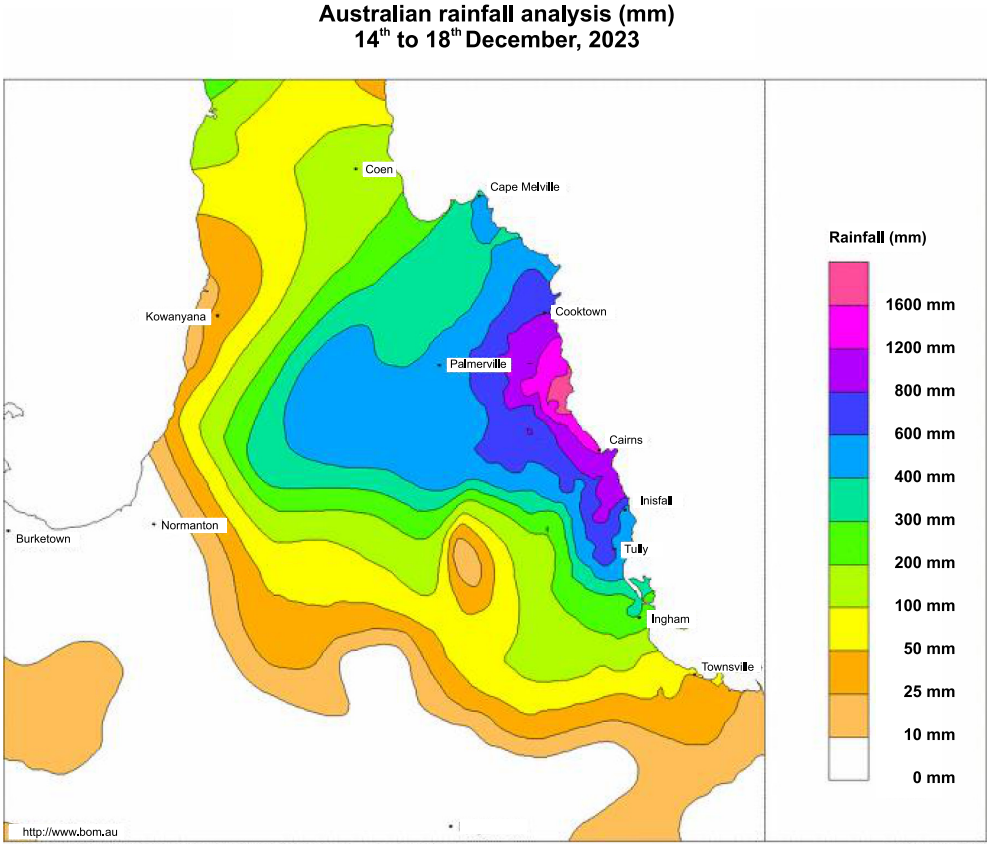

Fig. 2. Total rainfall (mm) recorded over the 5-d period of December 14th to 18th, 2023, in Queensland, Australia. Courtesy Australian Bureau of Meteorology.

global climate model historical simulations is then applied to the future climate (SSP3-7.0) simulations.

2. Results

The annual exceedance frequencies of storm total rainfall at Cairns from the ERA-5 downscaling and the downscalings of the global model fields for the historical and future climate periods are shown in Fig. 3. The frequency of storm total rainfall exceeding 1 m is highlighted for the global model means.

First, note that the rainfall frequencies from storms downscaled from ERA5 reanalyses align well with those from historical global model simulations up to about 2 m of rain, but are on the low side of the range of global model historical simulations for larger rainfall totals (but remain within a SD among the models).

At 1 m of rainfall, the distributions of frequencies among the models are well separated between the historical and future climate simulations, but naturally the scatter among the global model-driven downscalings is larger in the future climate, reflecting uncertainty in climate change projections.

Based on multimodel means, the annual frequency of storm total rainfall exceeding 1 m at Cairns nearly triples from about 0.0079 to 0.0233 between 2000 and 2085, the mid-points of the two time periods. Interpolating linearly in time, the frequency of exceeding 1 m of storm total rain increases by more than 50% to about 0.012 (once in 83 y) between 2000 and 2023, when Jasper occurred.

The track and storm total rainfall of a synthetic tropical cyclone that produced a 100-y rainfall by the standards of the period 1985 to 2014 is shown in Fig. 4*A*, while a similar map pertinent to a 100-y rainfall event during the period 2071 to 2100 is displayed in Fig. 4*B*. (The color scales are identical between the two panels of Fig. 4, but differ from the scale used in Fig. 2).

Note that the particular event selected for the 2071 to 2100 period is moving faster than the particular track selected for the 1985 to 2014 period but produces substantially more rain near the coast than does the 1999 event. It also produces more rain inland, thanks in part to its faster motion, and an increasing amount toward the west coast, owing to some reintensifcation of the storm over the Gulf of Carpentaria.

We can break down the contributions to changing rainfall from changing storm frequency, upward motion, moisture, and duration as follows:

First, for each individual cyclone, define a 96-h window centered on the time of closest approach of the cyclone center to the point of interest (Cairns, in this case). The rainfall algorithm calculates the rainfall R at the point of interest according to

$$R = \int_{t_{beg}}^{t_{end}} \varepsilon_p w q* \, dt, \qquad [1]$$

Where ε_p is a precipitation efficiency, w is the cyclone's vertical velocity, q^* is the saturation specific humidity at 900 hPa, and the time integration begins and ends at t_{beg} and t_{end}, which are here taken to be 48 h before and after the time of closest approach. The rainfall algorithm, as described by Feldmann et al. (7), calculates contributions to w from storm dynamics, Ekman pumping, topography, and interaction with environmental shear.

We next define a weighted rainfall duration D as

$$D \equiv \frac{1}{w_{50}} \int_{t_{beg}}^{t_{end}} w dt, \qquad [2]$$

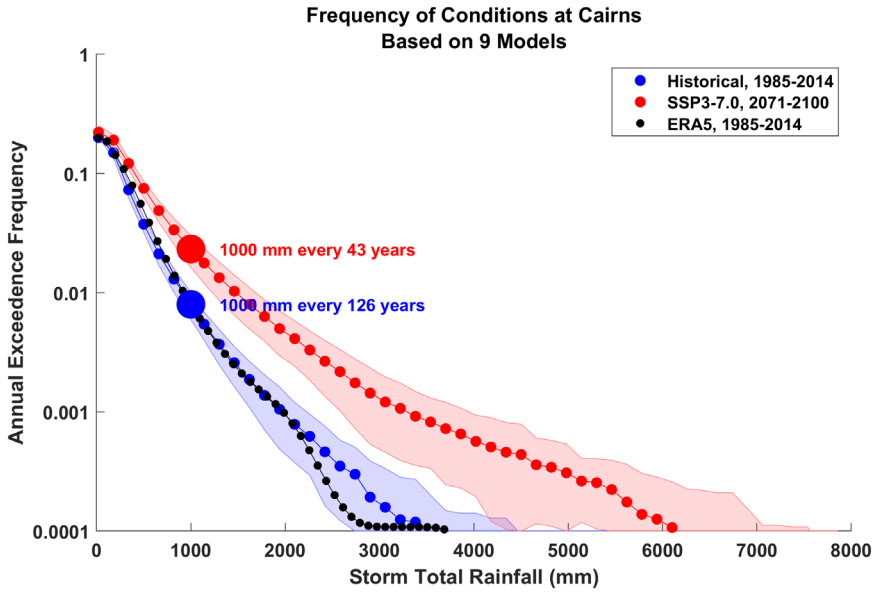

Fig. 3. Annual exceedance frequencies of storm total rainfall at Cairns for tropical cyclones downscaled from ERA5 (black), historical global model simulations (blue), and future climate global model simulations (red). The dotted colored curves show the multimodel mean exceedance frequencies, while the shading indicates one SD up and down among the nine climate models. The large dots show the multimodel mean annual frequencies of exceeding 1 m of storm total rainfall at Cairns, approximately that observed in Cyclone Jasper.

where w_{50} is the median of the positive values of w over the time interval of the integration. While there is some arbitrariness in this definition, it sensibly weights duration by the intensity of the rainfall, whose variability is mostly owing to variability in w.

The mean moisture content over the duration of the event at the point of interest is here defined

$$Q \equiv \frac{\int_{t_{beg}}^{t_{end}} wq * dt}{\int_{t_{beg}}^{t_{end}} wdt}. \qquad [3]$$

Again, we weigh moisture variability by the vertical velocity. In practice, since low-level temperature does not usually vary much over the course of an event, Q as defined above will usually be close to the time average saturation specific humidity at 900 hPa.

With these definitions, and taking ε_p as constant over the duration of the event, Eq. **1** becomes

$$R = \varepsilon_p QDw_{50}, \qquad [4]$$

and therefore

$$log\,(R) = log\,(\varepsilon_p) + log\,(Q) + log\,(D) + log\,(w_{50}). \qquad [5]$$

Note that the choice of the median of the positive values of vertical velocity is somewhat arbitrary. This affects the partitioning into duration and intensity but not the sum of the last two terms in Eq. **5**; consequently, the other terms in Eq. **5** and the effect of changing storm frequency are not affected by the choice. We will return to the choice of the intensity definition shortly.

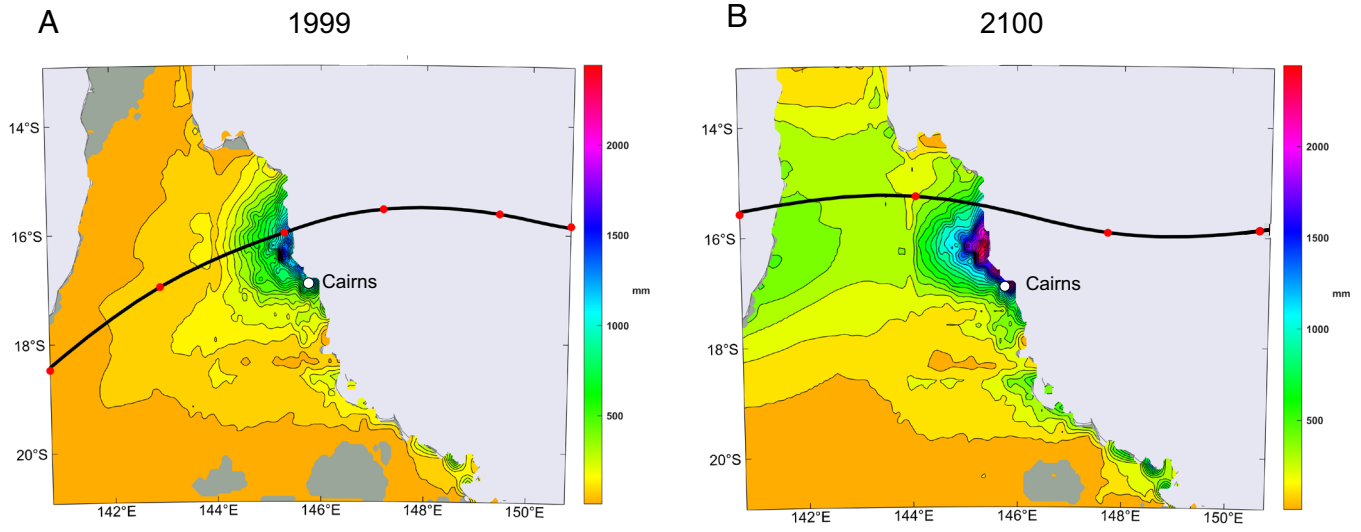

Fig. 4. Storm total rainfall for a representative 100-y storm in (*A*) 1999 and (*B*) 2100 under socioeconomic pathway SSP3-7.0. The color scales are the same for both maps, though they differ from that used to create Jasper's rainfall map (Fig. 2). The tracks of the cyclone centers are shown black with red dots showing 00 GMT positions. The white dot shows the location of Cairns.

Given this decomposition, we follow this procedure:

1. Calculate, as usual, the storm total rainfall for each event in the set.
2. Sort the events from largest to smallest storm total rainfall
3. Calculate the exceedance frequency of each event from the ordered list and from the overall frequency.
4. For all storms whose frequency is less than a specified threshold (here, one in 200 y), calculate a frequency-weighted average of each term on the right side of Eq. **5**.
5. Now repeat the above for the future climate state. Do this twice: Once holding the overall frequency at the historical climate level and the second time letting the overall frequency equal its value in the future climate.
6. Calculate the changes in the values of the terms on the right side of Eq. **5** from the historical to the future climate, holding frequency constant, and from the future climate with the historical climate frequency to the future climate with the future climate frequency.
7. Find the mean and variation of the results of steps 1 to 6 among the nine climate models.

In applying this procedure, we do not include changes in the precipitation efficiency; nor were such changes included in the downscaling. The results are displayed in Fig. 5*A*. Somewhat surprisingly, the increase in rainfall is dominated by increasing cyclone intensity, but with a large intermodel spread in that contribution. The next most important change is the increase in moisture, which has less uncertainty, probably because there is not much intermodel spread in the increase of temperature. The contribution from changing storm frequency is small, and there is a slightly negative contribution from duration, though with large uncertainty. We caution that this breakdown of contributions to changing rainfall may be quite specific to the choice of location and so these results should not necessarily be generalized to other places.

The effect of the choice of intensity definition is explored in Fig. 5*B*, where instead of defining intensity by the median of the positive vertical velocities over the duration of each event at Cairns, we define it by the mean over the positive values. (Examination of Eq. (**2**) shows that the duration in this case, if the vertical velocity is always positive, is just $t_{end} - t_{beg}$.) The changes of the logarithms of the frequency and moisture factors, as well as the total, remain unchanged, but the partitioning between duration and intensity differs. We now see a decided increase in duration, with little scatter among the models, and a smaller increase in intensity, now comparable to the effect of increasing moisture.

Regardless of the exact choice of intensity definition, there can be little question that increasing intensity contributes appreciably to increasing precipitation in the tropical cyclones affecting Cairns. Fig. 6 shows the annual exceedance frequency of the maximum wind speed of storms while they are within 150 km of Cairns. The overall frequency in the future climate state is held equal to that of the historical climate in constructing this graph, to focus attention on intensity alone. The increase in intensity is substantial, particularly for the low-frequency, high-intensity events. It is notable that this increase in intensity was not found in the Southwestern Pacific in a global downscaling conducted by the author (24). Although that study downscaled some of the same models used here, it pertained to simulations in which CO_2 concentrations were increased at a rate of 1% y^{-1}, so the response was fully transient, unlike the SSP3-7.0 pathway. Knutson et al. (25) also found slightly increasing intensity in the southwestern Pacific region, but that review was dominated by studies using direct general circulation model (GCM) simulations of tropical cyclones that were under-resolved. In their study, Dixon et al. (17) applied the same downscaling technique used here to five CMIP5-generation global climate models and found that three of these had increasing maximum wind speed near the Great Barrier Reef by the end of the century.

The important contribution of changing intensity to changing tropical cyclone rainfall was pointed out by Liu et al. (26) who explored changes in tropical cyclone rainfall over the global ocean using a high-resolution climate model. The model percentage changes in storm rainfall were roughly twice those predicted based on moisture alone, through the Clausius–Clapeyron equation, roughly consistent with Fig. 5 (comparing the total change to the change due to moisture alone).

One advantage of the downscaling used here is that storm intensity is not limited by numerical resolution, because the dynamical intensity model (27) is phrased in angular momentum coordinates, which yield increasing spatial resolution in the core of the storm as it intensifies. State-of-the-art global climate model grid spacings of around 25 km, such as used by Liu et al. (26) and Reed et al. (28), cannot resolve features much less than around 100 km in scale, still inadequate to resolve the cores of tropical cyclones (29). Such

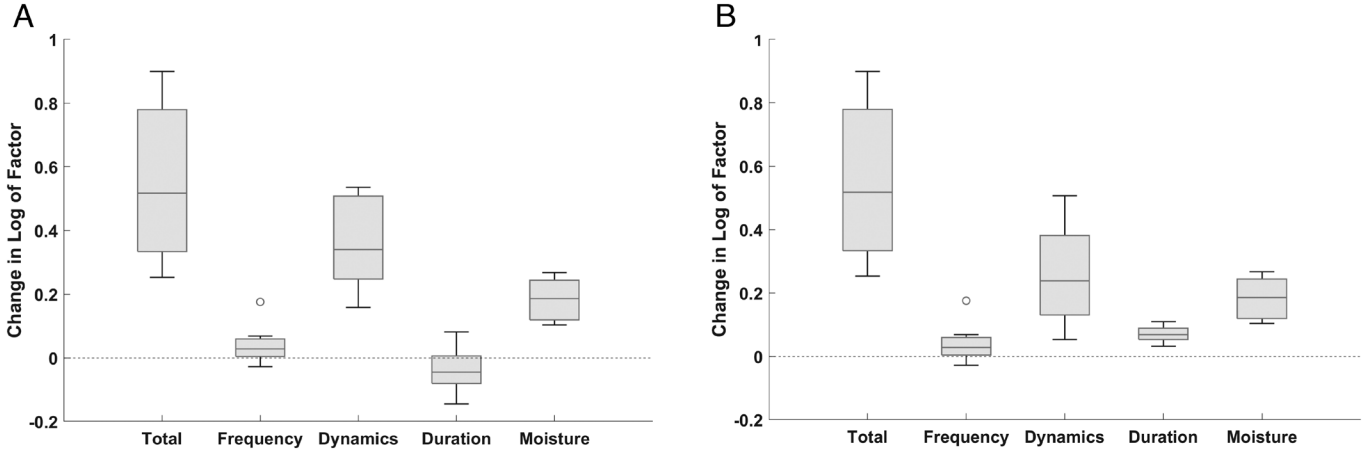

Fig. 5. (*A*) Changes from the historical to the future periods in the logarithms of the various contributions to storm total rainfall at 200-y return periods, as given by ref. 5. "Dynamics" refers to the vertical motion contribution. The boxes span from the lower to the upper quartiles of the distribution among the nine models, and the horizontal line represents the multimodel median. Outliers, defined as models more than 1.5 times the interquartile distance from the median, are displayed as small circles, and the whiskers extend from the lowest to the highest value among the nine models, excluding outliers. (*B*) as in (*A*) but defining the intensity by the mean, rather than the median, of positive values of vertical velocity over the duration of each event at Cairns.

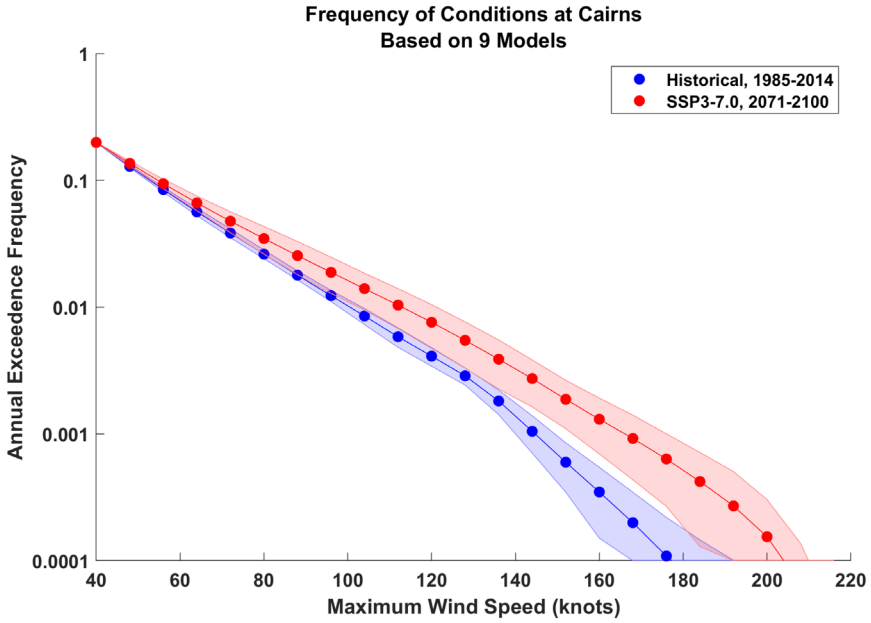

Fig. 6. Annual exceedance frequency of the maximum wind speed at Cairns based on 27,000 events between 1985 and 2014, and the same number of events between 2071 and 2100, downscaled from historical and SSP3-7.0 simulations by the nine climate models. The dots and thin lines show the multimodel means and the shading spans one SD up and down among the nine climate models. The overall frequency of future events has been kept equal to that of historical events.

models are also too expensive to use to explore tropical cyclone risk at individual points, where long integrations would be necessary for statistically robust risk assessments. Purely statistical downscaling (e.g., ref. 30) trained on future cyclones simulated by even high-resolution climate models also suffers from the inadequate resolution in such models.

3. Summary

Cyclone Jasper's devastating floods in Queensland remind us that the deleterious effects of climate change are felt primarily through extreme events which, owing to their sensitivity to climate, also serve as canaries in the mine of climate change. Civilization, from our general awareness of weather threats to specific building codes and property insurance premiums, is finely adapted to the comparatively stable climate we have enjoyed since the beginning of the Holocene. A rapid shift in that climate is underway, and the pace of our adaptation is too slow to prevent the large increases in damage and human suffering that ensue when once rare events become almost common. The evidence presented here suggests that the probability of a rainfall event of Jasper's magnitude has already increased by around 50% since the beginning of this century and is likely to double between now and the century's end. One can argue about the appropriate mix of adaptation to and mitigation of climate change, but setting policies, from building codes to insurance premiums to disaster preparedness, as though climate were stable should not be an option in a well-functioning civilization.

While the cost of climate change is felt primarily in extreme events that often occur on small scales, it is far easier to model climate on a global scale and look to proxies of local weather extremes or hope that the behavior of severely under-resolved local events is being correctly handled by global models. But to estimate the true risk of climate change, we must find improved ways of downscaling global climate that are based on physics rather than statistics alone and which can be used directly to estimate climate damages. In this way, climate science can serve as a more rational basis for society to deal with climate change.

Data, Materials, and Software Availability. All synthetic tropical cyclone data used in this study are available in netcdf format at https://zenodo.org/doi/10.5281/zenodo.10798333 (31). We ask that users of this data to not redistribute the data but rather refer other interested parties to this repository.

ACKNOWLEDGMENTS. K.E. gratefully acknowledges very helpful reviews by Michael Mann and Hamish Ramsay. He was supported by the NSF under grant 2202785.

1. D. Nicholson, Cyclone Jasper damage bill estimated to hit $1 billion. *The Cairns Post* (2023). https://www.cairnspost.com.au/news/cairns/more-assessors-on-the-ground-in-fnq-to-aid-recovery-from-cyclone-jasper/news-story/70a712eb54756195c16c347986cd37d8. Accessed 2 January 2024.
2. S. Turton, Cyclone Jasper and climate change. *Greenpeace* (2023). https://www.greenpeace.org/aotearoa/story/cyclone-jasper-and-climate-change/#:~:text=Queensland's record-breaking floods are, thousands of people to evacuate. Accessed 2 January 2024.
3. K. A. Emanuel, S. Ravela, E. Vivant, C. Risi, A statistical-deterministic approach to hurricane risk assessment. *Bull. Am. Meteor. Soc.* **19**, 299–314 (2006).
4. K. Emanuel, R. Sundararajan, J. Williams, Hurricanes and global warming: Results from downscaling IPCC AR4 simulations. *Bull. Am. Meteor. Soc.* **89**, 347–367 (2008).
5. K. Emanuel, E. Rappaport, *Forecast Skill of a Simplified Hurricane Intensity Prediction Model* (American Meteorological Society, Boston, 2000), pp. 236–237.
6. K. R. Knapp, M. C. Kruk, D. H. Levinson, H. J. Diamond, C. J. Neumann, The International Best Track Archive for Climate Stewardship (IBTrACS): Unifying tropical cyclone best track data. *Bull. Am. Meteor. Soc.* **91**, 363–376 (2010).
7. M. Feldmann, K. Emanuel, L. Zhu, U. Lohmann, Estimation of Atlantic tropical cyclone rainfall frequency in the United States. *J. Appl. Meteorol. Climatol.* **58**, 1853–1866 (2019).
8. K. Frieler *et al.*, Assessing the impacts of 1.5°C global warming–Simulation protocol of the Inter-Sectoral Impact Model Intercomparison Project (ISIMIP2b). *Geosci. Model Dev.* **10**, 4321–4345 (2017).
9. P. Irvine *et al.*, Halving warming with idealized solar geoengineering moderates key climate hazards. *Nat. Clim. Change* **9**, 295–299 (2019).
10. R. Marsooli, N. Lin, K. Emanuel, K. Feng, Climate change exacerbates hurricane flood hazards along US Atlantic and Gulf Coasts in spatially varying patterns. *Nat. Commun.* **10**, 3785 (2019).
11. A. Chen, K. A. Emanuel, D. Chen, C. Lin, F. Zhang, Rising future tropical cyclone-induced extreme winds in the Mekong River Basin. *Sci. Bull.* **65**, 419–424 (2020).
12. S. Lange *et al.*, Projecting exposure to extreme climate impact events across six event categories and three spatial scales. *Earth's Future* **8**, e2020EF001616 (2020).
13. P. D. Bates *et al.*, Combined modelling of US fluvial, pluvial and coastal flood hazard under current and future climates. *Water Resour. Res.* **57**, e2020WR028673 (2021).
14. W. Thiery *et al.*, Intergenerational inequities in exposure to climate extremes. *Science* **374**, 158–160 (2021).
15. M. J. U. Khan *et al.*, Storm surge hazard over Bengal delta: A probabilistic-deterministic modelling approach. *Nat. Hazards Earth Syst. Sci. Discuss.* **2021**, 1–30 (2021).

16. A. Gori, N. Lin, D. Xi, K. Emanuel, Tropical cyclone climatology change greatly exacerbates US extreme rainfall–surge hazard. *Nat. Clim. Change* **12**, 171–178 (2022), 10.1038/s41558-021-01272-7.
17. A. M. Dixon, M. Puotinen, H. A. Ramsay, M. Beger, Coral reef exposure to damaging tropical cyclone waves in a warming climate. *Earth's Future* **10**, e2021EF002600 (2022).
18. S. Meiler *et al.*, Intercomparison of regional loss estimates from global synthetic tropical cyclone models. *Nat. Commun.* **13**, 6156 (2022).
19. K. Emanuel, Assessing the present and future probability of Hurricane Harvey's rainfall. *Proc. Natl. Acad. Sci. U.S.A.* 114, 12681–12684 (2017), 10.1073/pnas.1716222114.
20. L. Zhu, S. M. Quiring, K. A. Emanuel, Estimating tropical cyclone precipitation risk in Texas. *Geophy. Res. Lett.* **40**, 6225–6230 (2013).
21. E. Vosper, D. Mitchell, K. Emanuel, Extreme hurricane rainfall affecting the Caribbean mitigated by the Paris agreement goals. *Environ. Res. Lett.* **15**, 104053 (2020).
22. L. Zhu, K. Emanuel, S. M. Quiring, Elevated risk of tropical cyclone precipitation and pluvial flood in Houston under global warming. *Environ. Res. Lett.* **16**, 094030 (2021).
23. H. Hersbach *et al.*, The ERA5 global reanalysis. *Q. J. R. Meteorol. Soc.* **146**, 1999–2049 (2020).
24. K. Emanuel, Response of global tropical cyclone activity to increasing CO2: Results from downscaling CMIP6 models. *J. Clim.* **34**, 57–70 (2020).
25. T. Knutson *et al.*, Tropical cyclones and climate change assessment: Part II: Projected response to anthropogenic warming. *Bull. Am. Meteorol. Soc.* **101**, E303–E322 (2020).
26. M. Liu, G. A. Vecchi, J. A. Smith, T. R. Knutson, Causes of large projected increases in hurricane precipitation rates with global warming. *npj Clim. Atmos. Sci.* **2**, 38 (2019).
27. K. A. Emanuel, The behavior of a simple hurricane model using a convective scheme based on subcloud-layer entropy equilibrium. *J. Atmos. Sci.* **52**, 3959–3968 (1995).
28. K. A. Reed, M. F. Wehner, C. M. Zarzycki, Attribution of 2020 hurricane season extreme rainfall to human-induced climate change. *Nat. Commun.* **13**, 1905 (2022).
29. R. Rotunno *et al.*, Large-eddy simulation of an idealized tropical cyclone. *Bull. Amer. Meteor. Soc.* **90**, 1783–1788 (2009).
30. N. Bloemendaal *et al.*, Generation of a global synthetic tropical cyclone hazard dataset using STORM. *Sci. Data* **7**, 40 (2020).
31. K. Emanuel, Data from "Cyclone Jasper's rains in the context of climate change." Zenodo. Available at https://zenodo.org/doi/10.5281/zenodo.10798333. Deposited 8 March 2024.